Supporting Information For

Nanoscale Insights into Ostwald Ripening of Clathrate Hydrates: A Correlative Atomic Force Microscopy and Molecular Dynamics Study

Total number of pages: 20

Total number of figures: 20

Total number of tables: 1

Total number of videos: 2

Contents of the Supplementary Material

S1. Additional Details for Simulation Models and Methods

Simulation Models

THF hydrate belongs to the SII-type hydrate, mainly composed of 5^{12} and $5^{12}6^4$ cages. THF hydrate nanoparticles with a diameter of 6 nm contain 3527 H_2O and 203 THF molecules. THF hydrate nanoparticles with a diameter of 4.5 nm contain 1557 H_2O and 91 THF molecules. THF hydrate nanoparticles with a diameter of 3 nm contain 481 H_2O and 33 THF molecules. The NP_{2THF} system contains 26,349 H_2O molecules and 294 THF molecules, while the NP_{3THF} system contains 26,349 H_2O molecules and 327 THF molecules. All force field parameters for H_2O and THF molecules in the systems are shown in Table S2. To distinguish between the different nanoparticles during analysis, each hydrate nanoparticle is assigned to either the D_6, $D_{4.5}$, or D_3 cluster based on its radial distance from the center of mass of the respective hydrate nanoparticle. To accurately evaluate the geometric properties of these irregular clusters, a dynamic tracking method is applied at each simulation frame. First, the specific IDs of the water molecules forming the hydrate cages are dynamically identified for each assigned THF hydrate nanoparticle. Subsequently, based on these extracted molecular IDs, the volume and surface area of each individual THF hydrate nanoparticle are computed using the gmx sasa algorithm within the GROMACS package. This approach provides a rigorous quantitative measure of the geometric evolution for each distinct hydrate phase. Cage identification based on the spatial distribution of the attributed molecules is performed, which categorizes the hydrogen bonded networks into specific cage types. During the analysis, a dynamic two-step protocol is employed to distinguish and track the different hydrate nanoparticles. First, the cage analysis algorithm is utilized to dynamically identify the specific IDs of all water and THF molecules that constitute intact clathrate hydrate cages at each simulation step. Any molecules that detach and dissolve into the bulk aqueous phase lose their clathrate cage structure and are therefore automatically excluded from this selection. Second, strictly among these identified cage-forming molecules, the dynamic centers of mass for the distinct solid clusters are calculated. The cage-forming molecules are then assigned to the D_6, $D_{4.5}$, or D_3 nanoparticles based on their spatial proximity to these dynamically updated centers. The volume and surface area of each irregular nanoparticle are subsequently evaluated based solely on the spatial distribution of these structurally intact, assigned molecules.

Simulation Methods

The geometry of the H_2O molecules is maintained by applying the SETTLE algorithm [1]. TIP4P-Ice [2] force fields were used for H_2O molecules. The TIP4P-Ice model was selected due to its demonstrated accuracy in predicting the phase equilibria and melting points of water-based crystalline structures, which is essential for maintaining the stability of the hydrate lattice at 258.15 K. This choice ensures that the simulations effectively capture the thermodynamic driving forces of Ostwald ripening while remaining consistent with the temperature conditions employed in the AFM experiments. The Lorentz-Berthelot mixing rules are used for describing the unlike interactions. The equations of motion were integrated according to the leapfrog algorithm with a 2.0 fs

timestep. The initial configurations were energy minimized by using the steepest descent algorithm. A pre-equilibrium simulation was performed for 2 ns, and the temperature was set to 258.15 K by controlling the v-rescale [3] algorithm, and the pressure was 1 bar by the Berendsen [4] algorithm. The isothermal-isobaric *NPT* ensemble balance for NP_{2THF} (100 ns) and NP_{3THF} (200 ns) systems was carried out at a constant temperature (T = 258.15 K) using Nosé-Hoover [5] temperature coupling, and at a constant pressure (P = 1 bar) using Parinello-Rahman [6] pressure coupling. To monitor the formation and coarsening process of THF hydrates, the cage analysis algorithm proposed by Jacobson et al. [7] is used to identify the seven cage types (5^{12}, $5^{12}6^2$, $5^{12}6^3$, $5^{12}6^4$, $4^15^{10}6^2$, $4^15^{10}6^3$, and $4^15^{10}6^4$). This algorithm systematically maps the hydrogen bond network to identify fundamental polygonal water rings, such as pentagons and hexagons. By analyzing the topological connectivity and spatial closure of these rings, the method enables the rigorous geometric classification of the resulting three-dimensional clathrate cavities. The selection of the TIP4P-Ice water model is based on its superior performance in reproducing the thermodynamic stability and phase equilibria of clathrate hydrates. This model provides a precise representation of the hydrogen bonded framework and accurately predicts the melting points and lattice constants of clathrate structures, which is critical for simulating the structural transformations observed in our experiments at 258.15 K. Furthermore, the guest molecules were modeled using the OPLS-AA force field to ensure robust compatibility with the water model and to facilitate an accurate description of the non-bonded interactions between the guest and the water cages. Detailed parameters for these models are provided in Table S1 of the Supporting Information. This combination of force fields has been previously validated for characterizing the interfacial properties and surface dynamics of gas hydrates, including the formation of the quasi-liquid layer.

Table S1. Parameters for the TIP4P/ice water model [2], TraPPE THF [8]. σ and ε are the Lennard-Jones parameters, in units of nm and kJ/mol, respectively; q is the partial charge of an atom in units of elementary charge (e); m is the atomic mass in units of g/mol.

atom	ε / [kJ/mol]	σ / [nm]	q / [e]	m / [g/mol]
H_2O				
O (MW)	0	0	-1.1794	0
O	0.8822	0.31668	0	16
H	0	0	0.5897	1.008
THF				
O	1.579747	0.22	-0.41	15.9994
CA	0.46810	0.388	0.16	14.027
CB	0.46810	0.388	0.045	14.027

S2. Supporting Figures

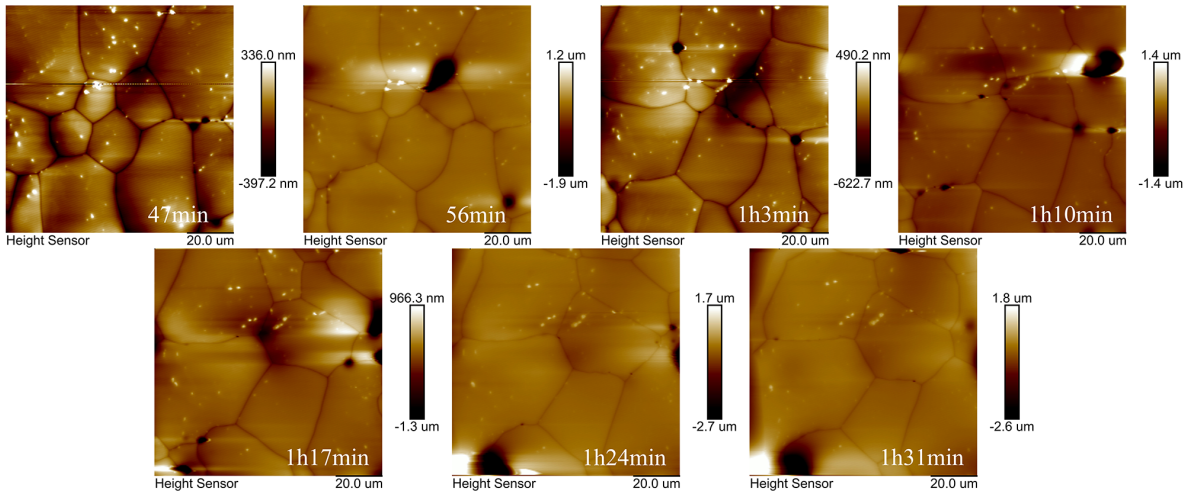

Figure S1. The time evolution of surface height images of ice surfaces.

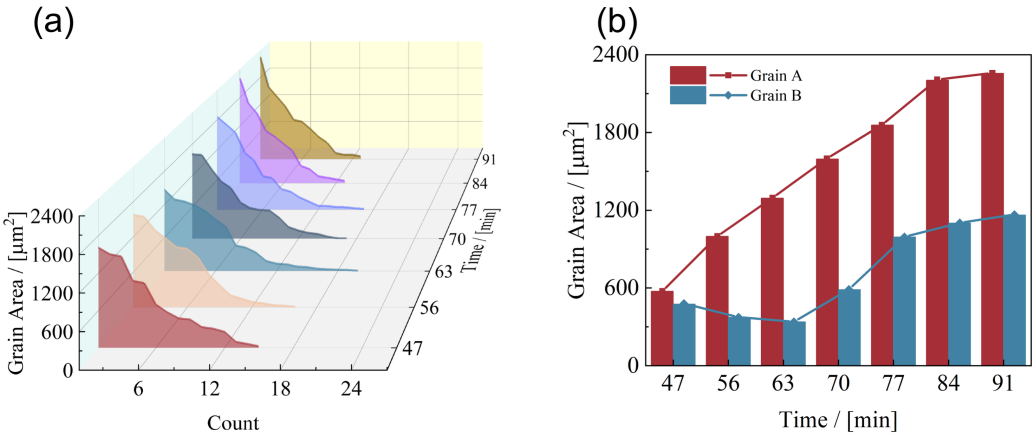

Figure S2. (a) The evolution of the grain area and population of the ice. (b) The evolution of grain areas for three different ice grains.

Following the methodology outlined in the main text, ice samples are prepared on freshly cleaved mica substrates under controlled conditions (environmental dew point < -55°C). Surface topography of the ice is acquired in tapping mode using AFM, with continuous imaging of the same microregion over approximately 1.5 hours (Figure S1). The ice grains exhibit distinct morphological features, predominantly irregular pentagons or polygons, with sharp grain boundaries. Differences in 2D height profiles arose from variations in grain size and population, analogous to the THF hydrate system.

For quantitative analysis, grain areas and counts are extracted from sequential AFM scans (Figure S2(a-b)). Similar to THF hydrates, ice grains exhibit dynamic coarsening behavior, *i.e.*, large grains progressively expand, while small ones diminish. This observation further supports the universality of Ostwald ripening in crystalline systems under interfacial instability. The consistency between THF hydrates and ice highlights the critical role of Ostwald ripening in mediating recrystallization processes.

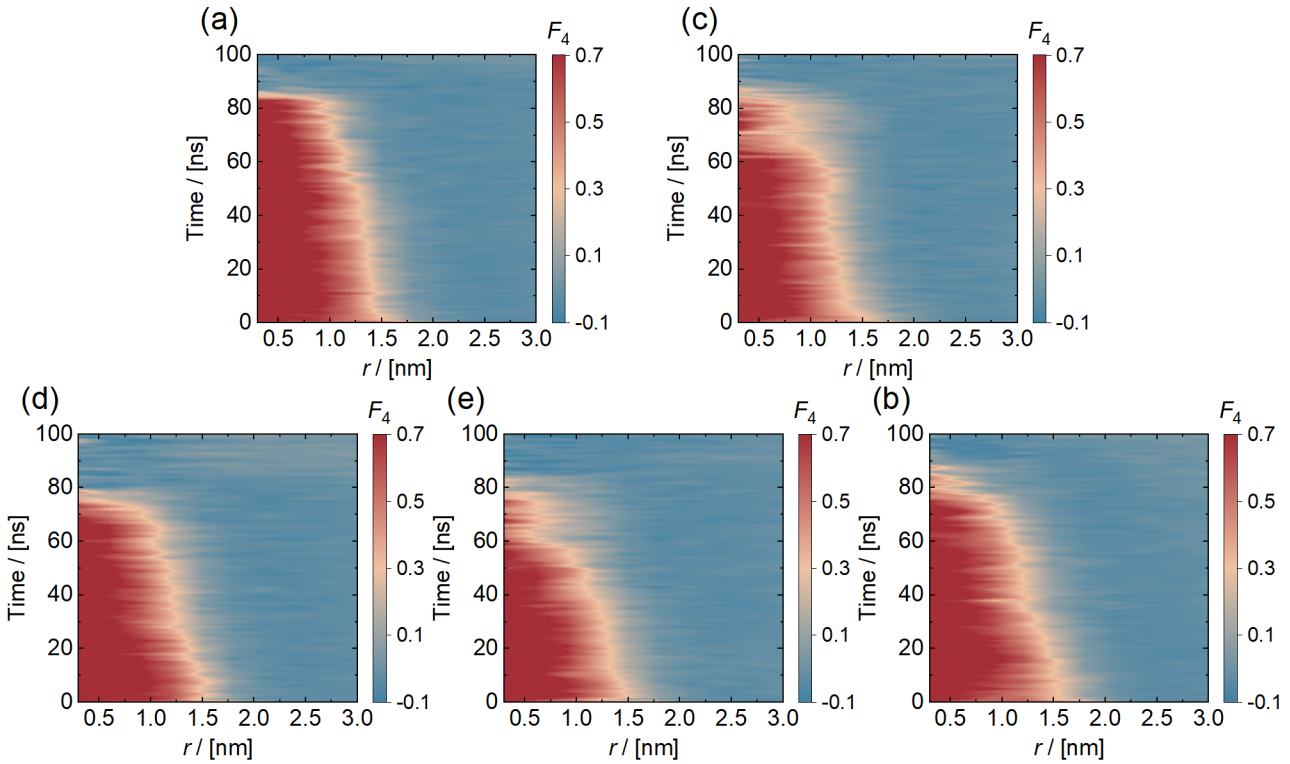

Figure S3. Time evolution of the F_4 from the center of the $D_{4.5}$ hydrate nanoparticle for the NP_{2THF} repeated systems, *i.e.*, (a) Run1, (b) Run2, (c) Run3, (d) Run4, and (e) Run5. The r = 0 nm represents the center of the hydrate nanoparticle, while sampling was averaged for 1 ns.

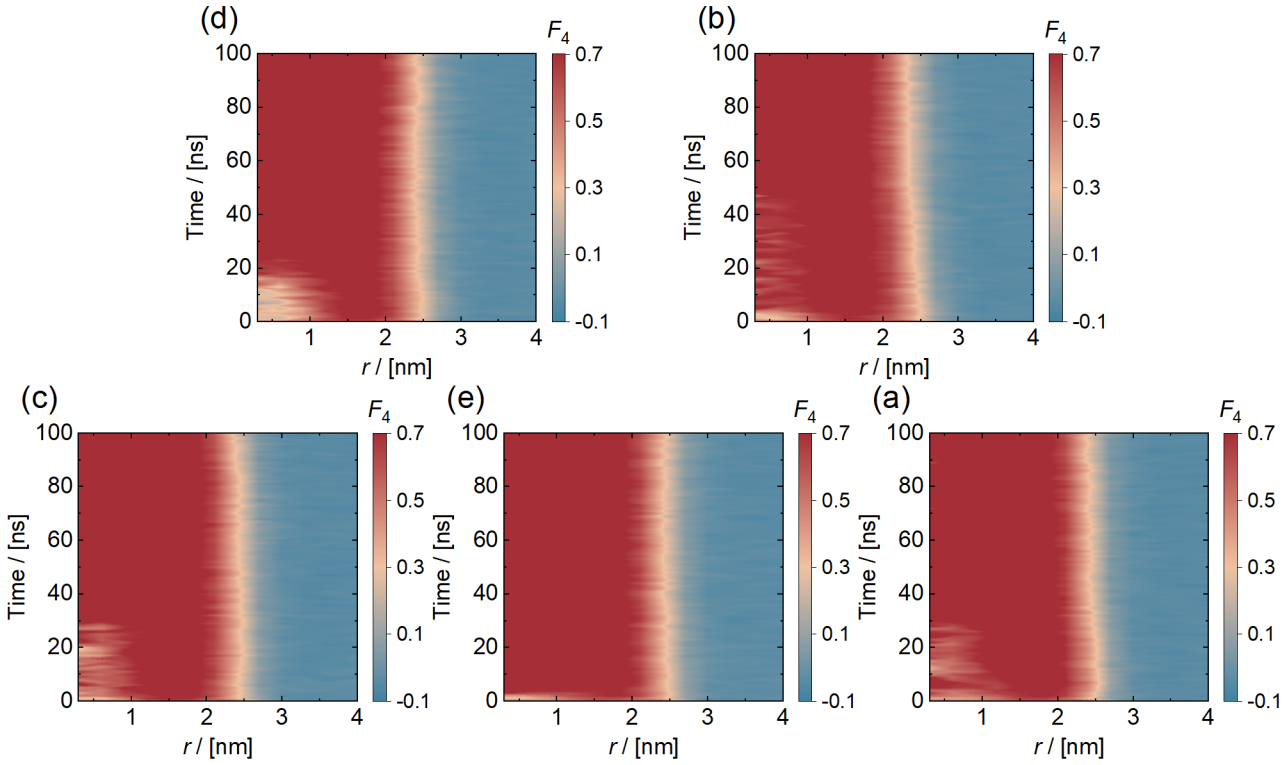

Figure S4. Time evolution of the F_4 from the center of the D_6 hydrate nanoparticle for the NP_{2THF} repeated systems, *i.e.*, (a) Run1, (b) Run2, (c) Run3, (d) Run4, and (e) Run5. The r = 0 nm represents the center of the hydrate nanoparticle, while sampling was averaged for 1 ns.

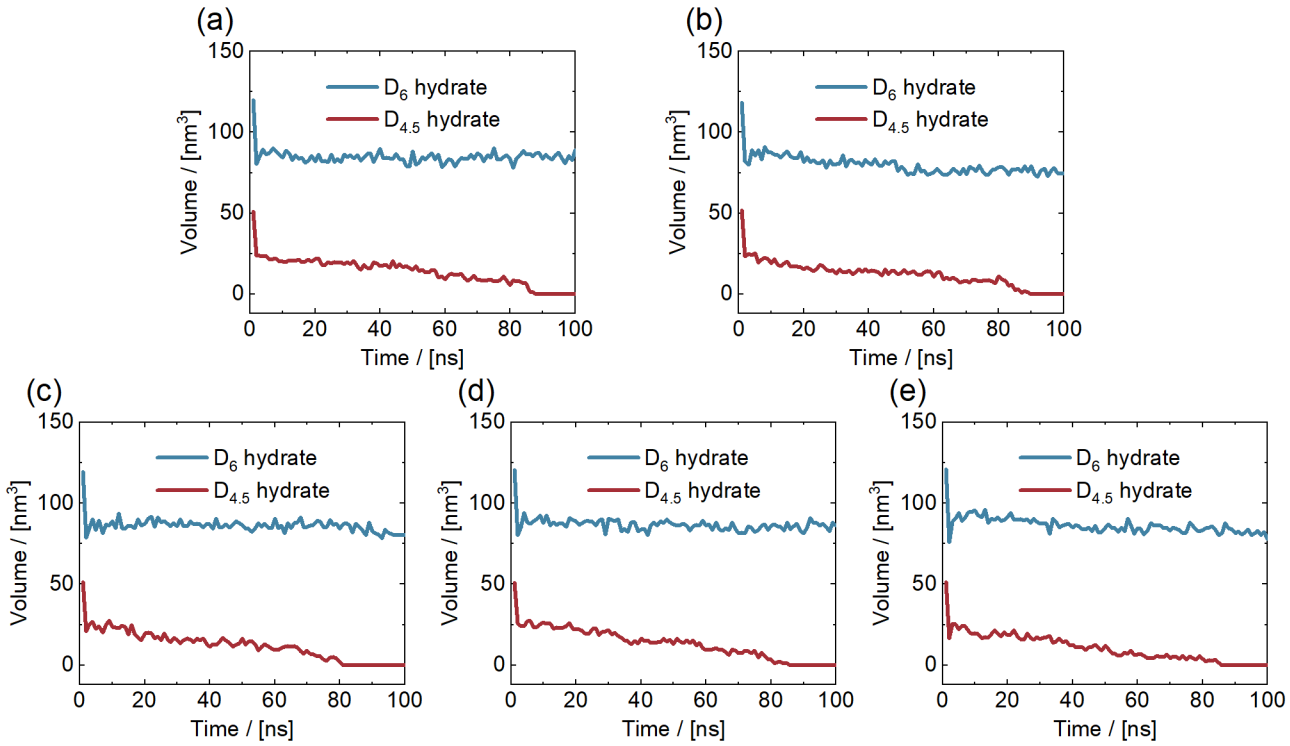

Figure S5. Time evolution of the volume of the $D_{4.5}$ and D_6 hydrate nanoparticles for the NP_{2THF} repeated systems, *i.e.*, (a) Run1, (b) Run2, (c) Run3, (d) Run4, and (e) Run5.

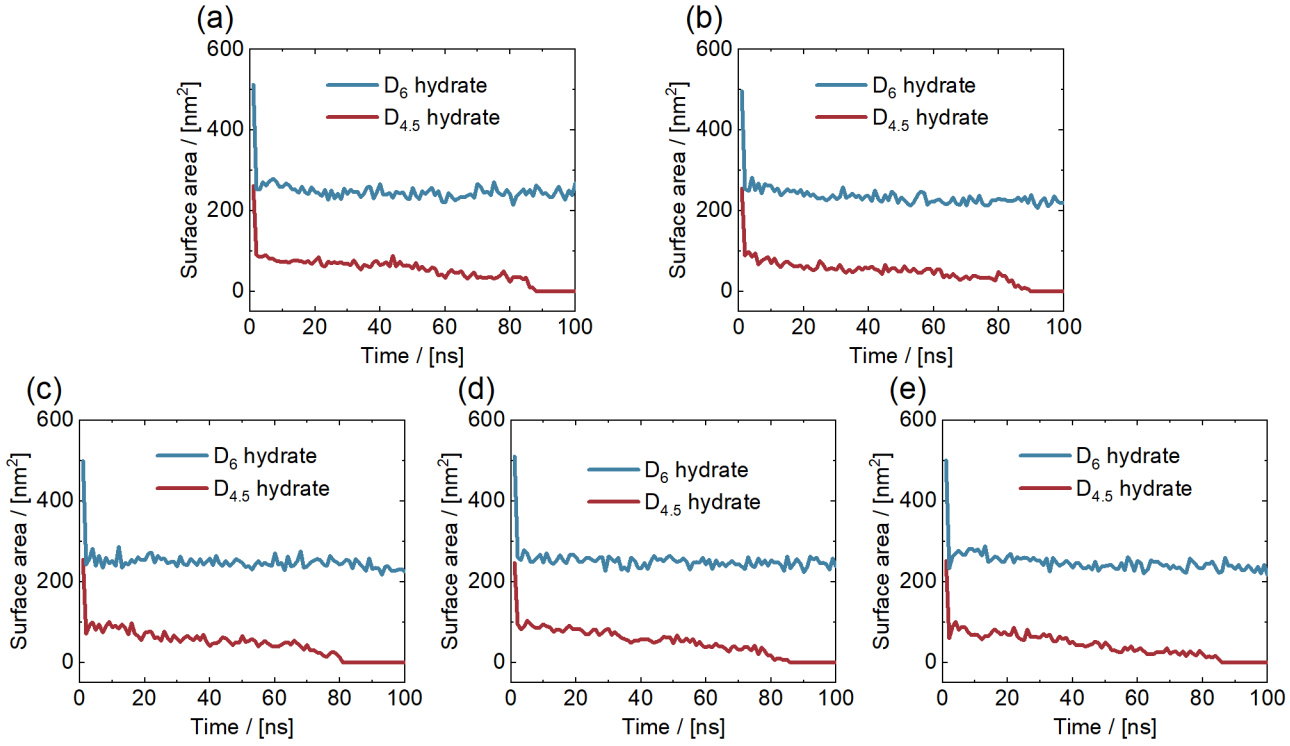

Figure S6. Time evolution of the surface area of the $D_{4.5}$ and D_6 hydrate nanoparticles for the NP_{2THF} repeated systems, *i.e.*, (a) Run1, (b) Run2, (c) Run3, (d) Run4, and (e) Run5.

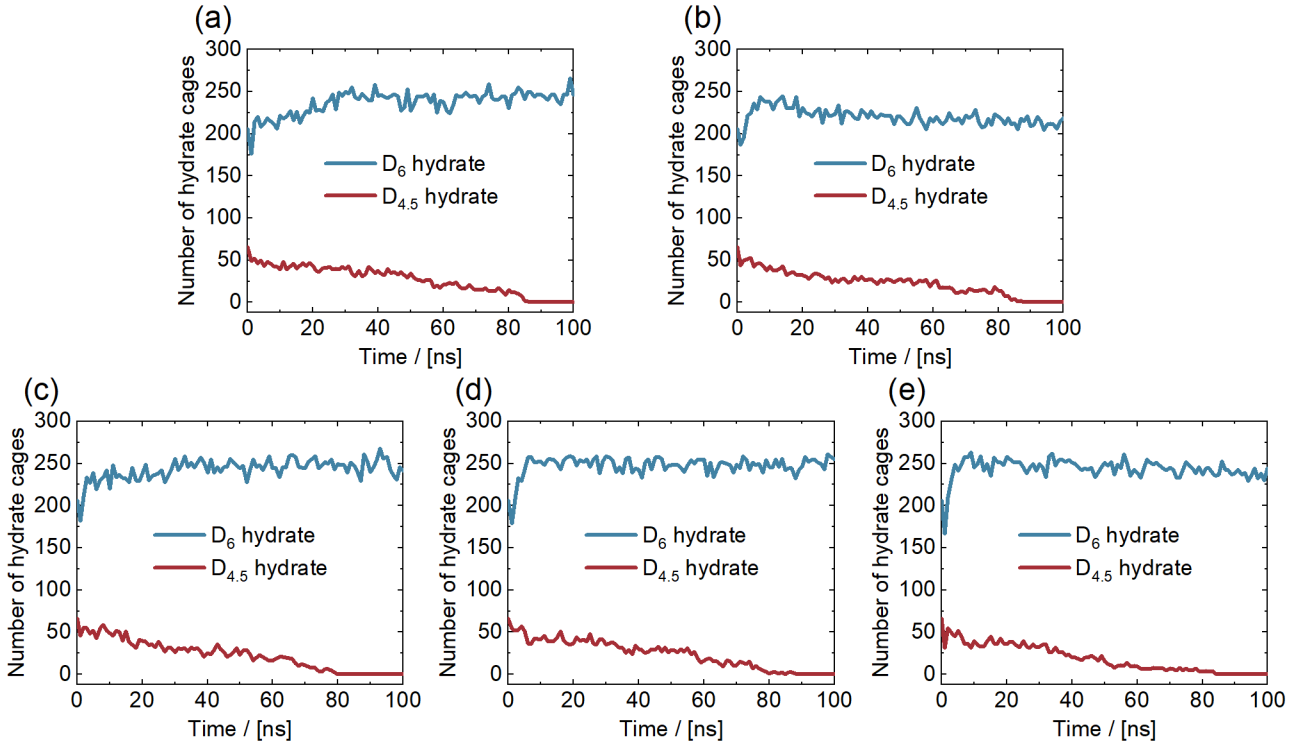

Figure S7. Time evolution of the number of cages in the $D_{4.5}$ and D_6 hydrate nanoparticles for the NP_{2THF} repeated systems, *i.e.*, (a) Run1, (b) Run2, (c) Run3, (d) Run4, and (e) Run5.

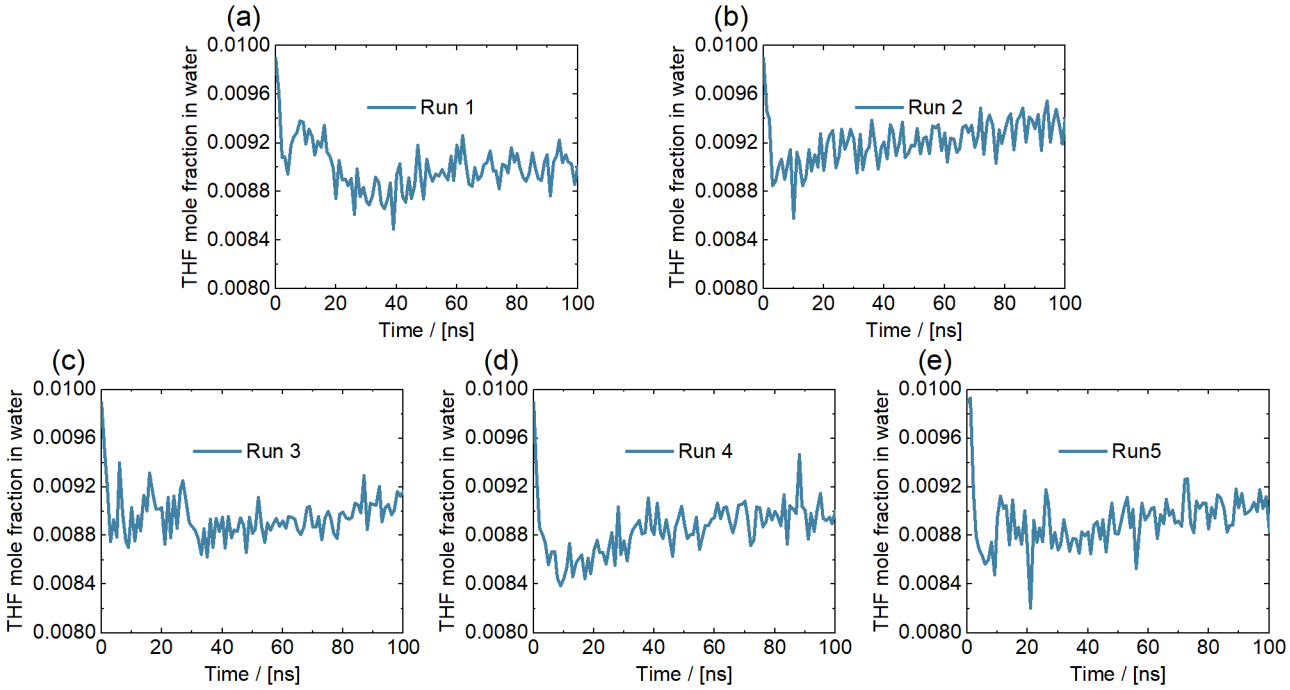

Figure S8. Time evolution of the THF mole fraction in water for the NP_{2THF} repeated systems, *i.e.*, (a) Run1, (b) Run2, (c) Run3, (d) Run4, and (e) Run5.

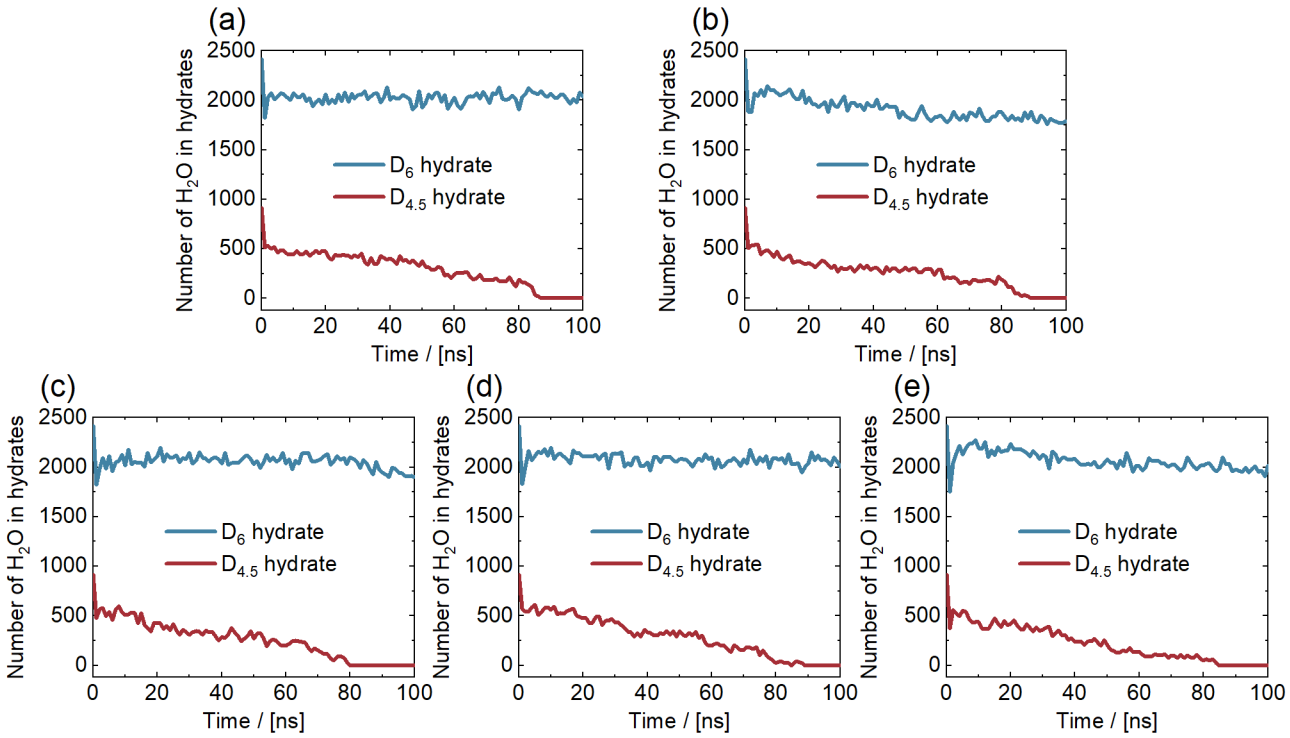

Figure S9. Time evolution of the number of H_2O molecules in the $D_{4.5}$ and D_6 hydrate nanoparticles for the NP_{2THF} repeated systems, *i.e.*, (a) Run1, (b) Run2, (c) Run3, (d) Run4, and (e) Run5.

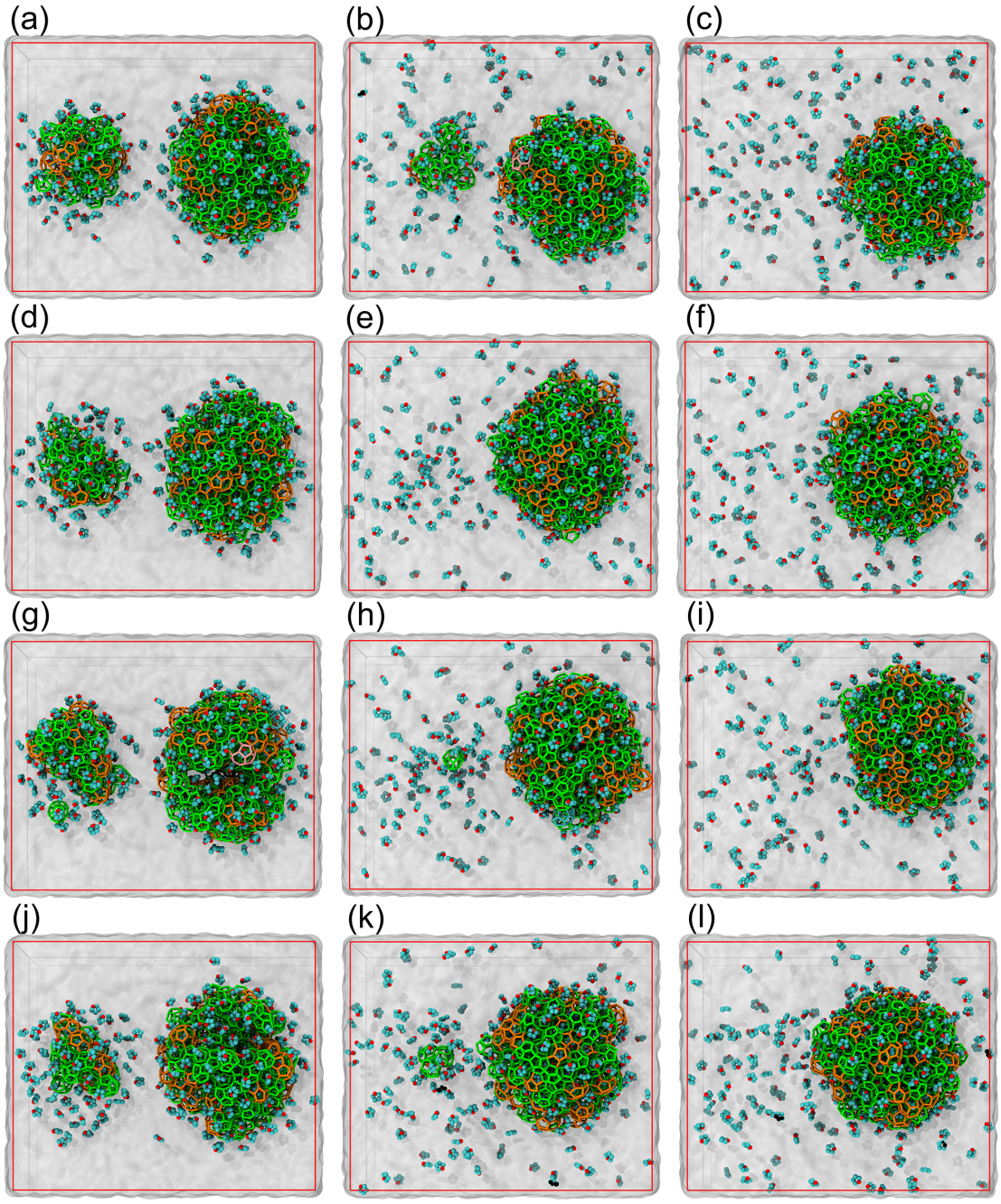

Figure S10. Simulation snapshots showing the coarsening process of THF hydrates for the NP_{2THF} repeated systems, *i.e.*, (a-c) Run2, (d-f) Run3, (g-i) Run4, and (j-l) Run5 at different simulation times (1 ns, 80 ns, and 100 ns). THF is displayed as cyan (C atom) and red (O atom). Bonds of different colours represent seven types of hydrate cages, *i.e.*, green for 5^{12}, and orange for $5^{12}6^4$.

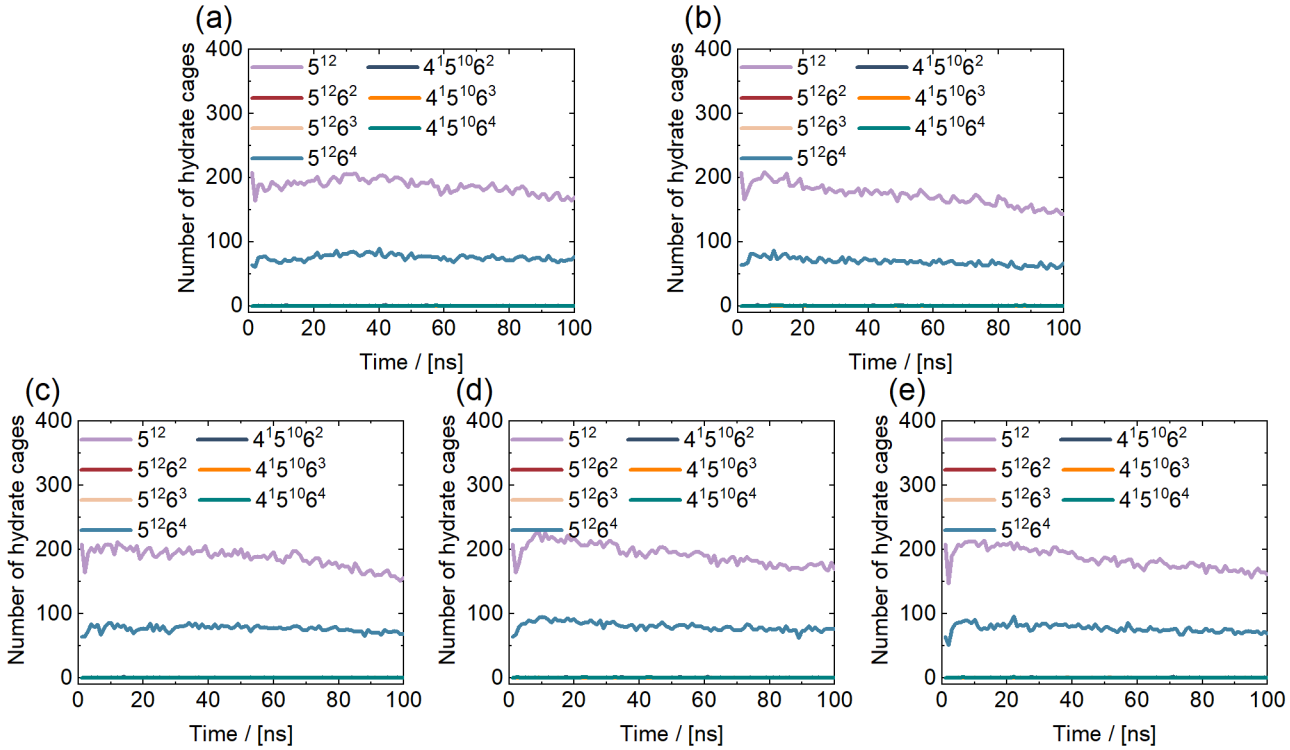

Figure S11. Time evolution of the number of hydrate cages for the NP_{2THF} repeated systems, *i.e.*, (a) Run1, (b) Run2, (c) Run3, (d) Run4, and (e) Run5.

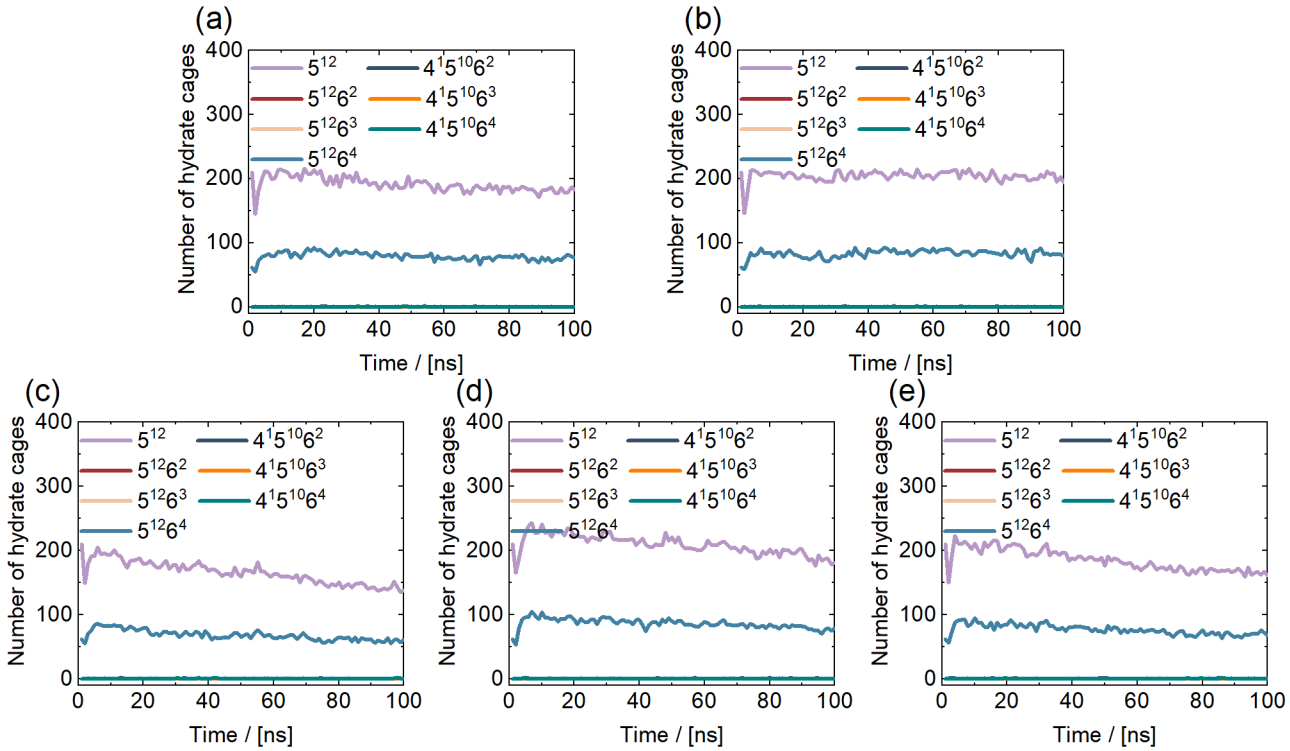

Figure S12. Time evolution of the number of hydrate cages for the NP_{3THF} repeated systems, *i.e.*, (a) Run1, (b) Run2, (c) Run3, (d) Run4, and (e) Run5.

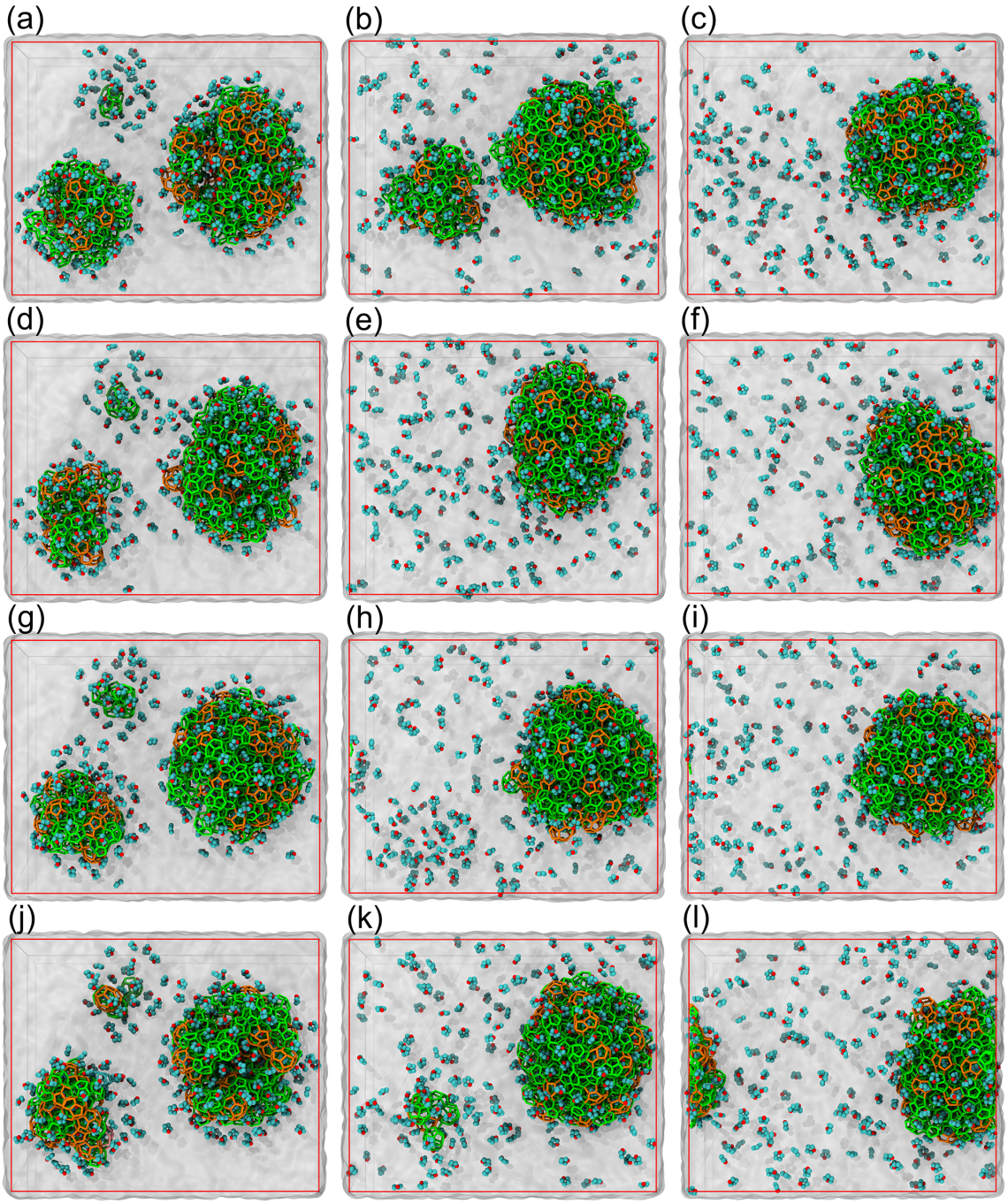

Figure S13. Simulation snapshots showing the coarsening process of THF hydrates for the NP_{3THF} repeated systems, *i.e.*, (a-c) Run2, (d-f) Run3, (g-i) Run4, and (j-l) Run5 at different simulation times (1 ns, 80 ns, and 100 ns). THF is displayed as cyan (C atom) and red (O atom). Bonds of different colours represent seven types of hydrate cages, *i.e.*, green for 5^{12}, and orange for $5^{12}6^4$.

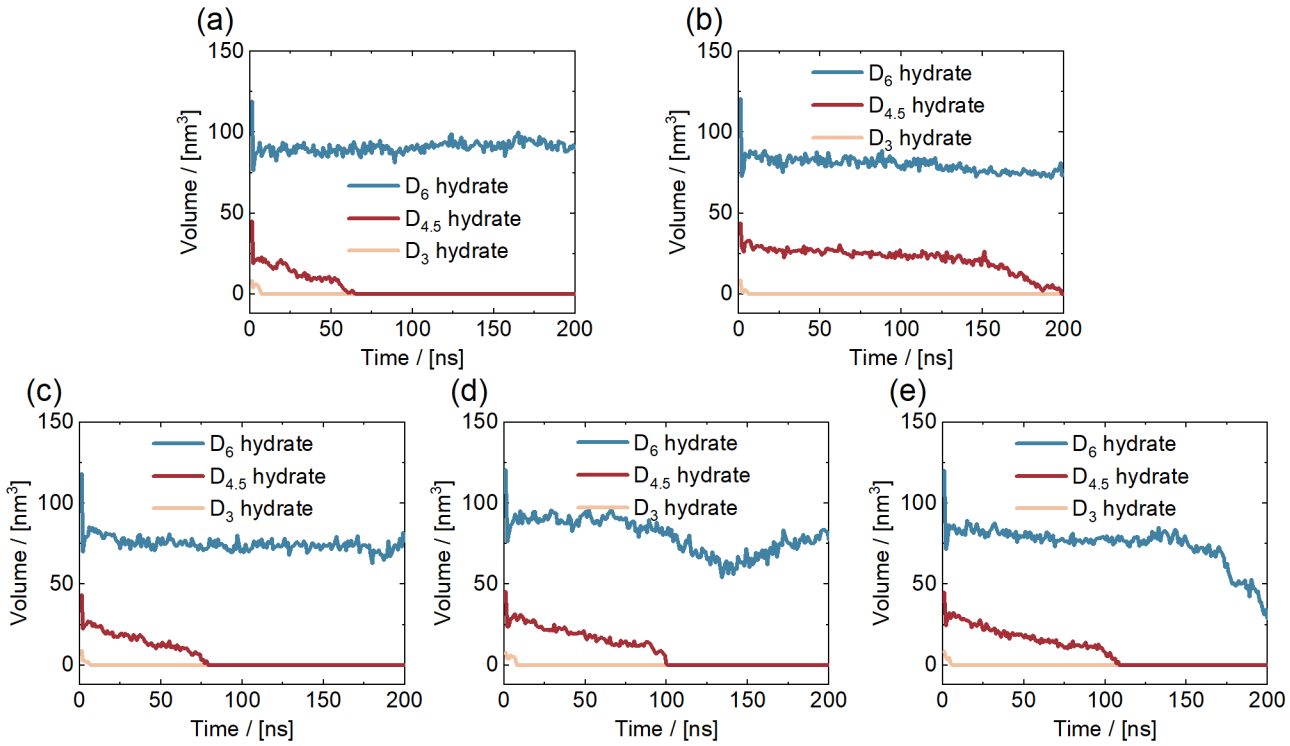

Figure S14. Time evolution of the volume of the $D_{4.5}$ and D_6 hydrate nanoparticles for the NP_{3THF} repeated systems, *i.e.*, (a) Run1, (b) Run2, (c) Run3, (d) Run4, and (e) Run5.

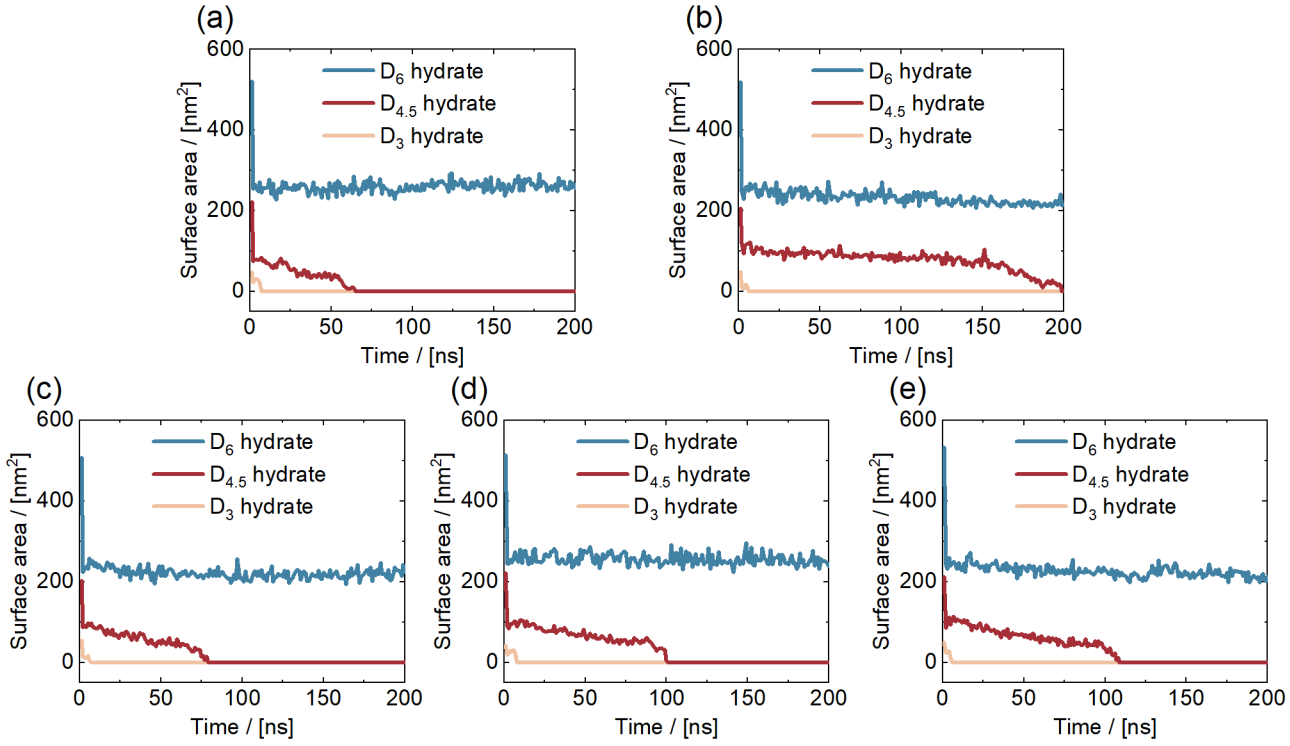

Figure S15. Time evolution of the surface area of the $D_{4.5}$ and D_6 hydrate nanoparticles for the NP_{3THF} repeated systems, *i.e.*, (a) Run1, (b) Run2, (c) Run3, (d) Run4, and (e) Run5.

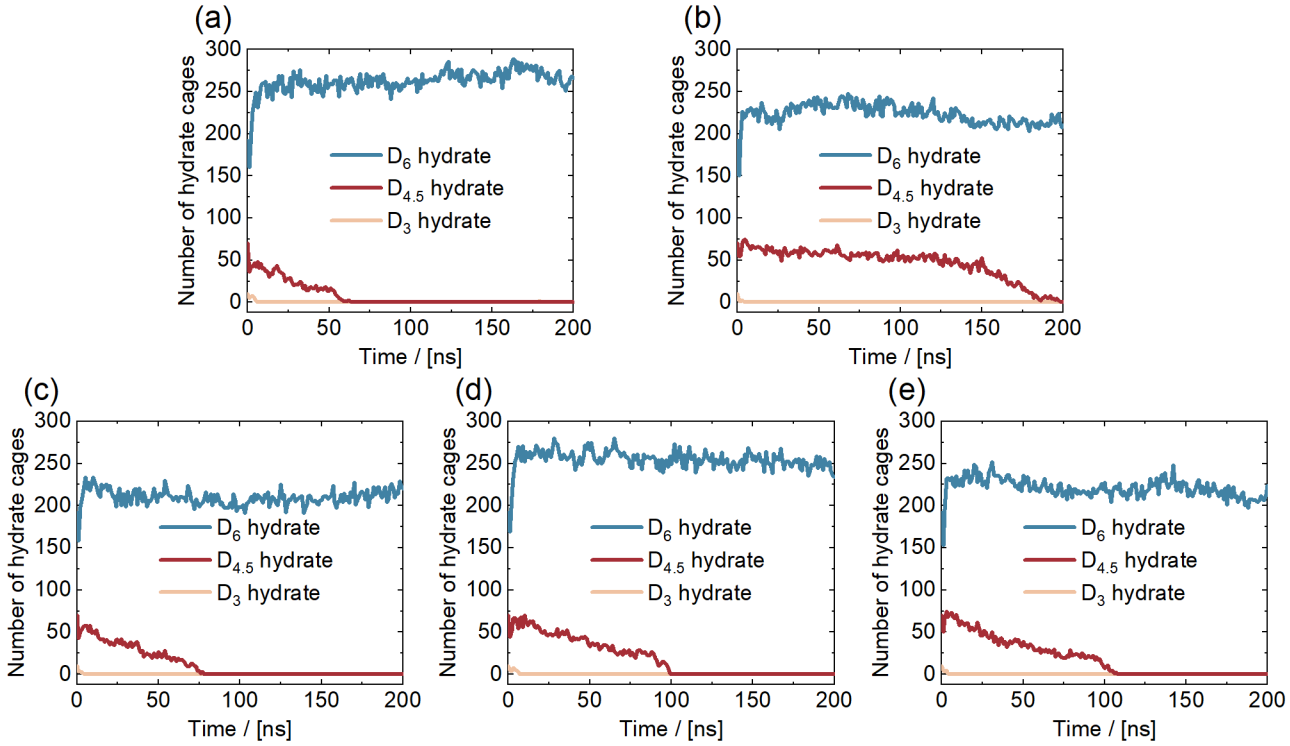

Figure S16. Time evolution of the number of cages in the $D_{4.5}$ and D_6 hydrate nanoparticles for the NP_{3THF} repeated systems, *i.e.*, (a) Run1, (b) Run2, (c) Run3, (d) Run4, and (e) Run5.

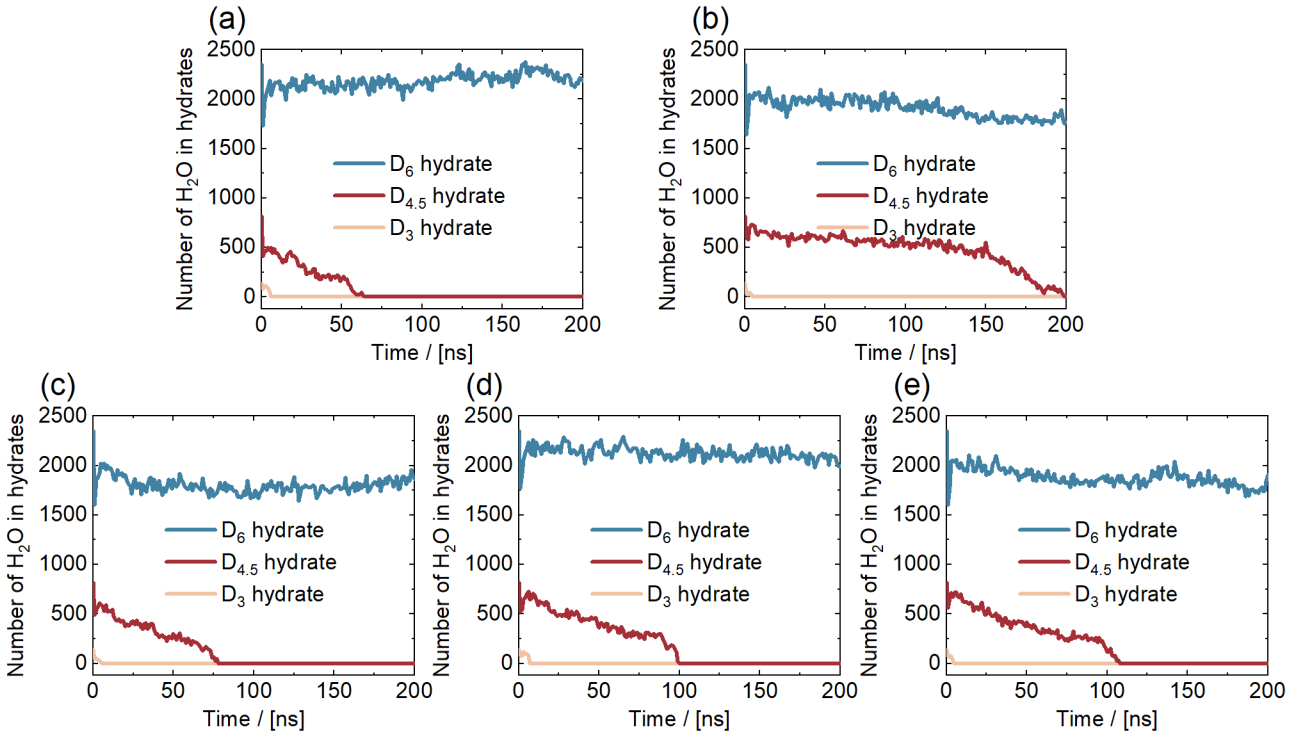

Figure S17. Time evolution of the number of H_2O molecules in the $D_{4.5}$ and D_6 hydrate nanoparticles for the NP_{3THF} repeated systems, *i.e.*, (a) Run1, (b) Run2, (c) Run3, (d) Run4, and (e) Run5.

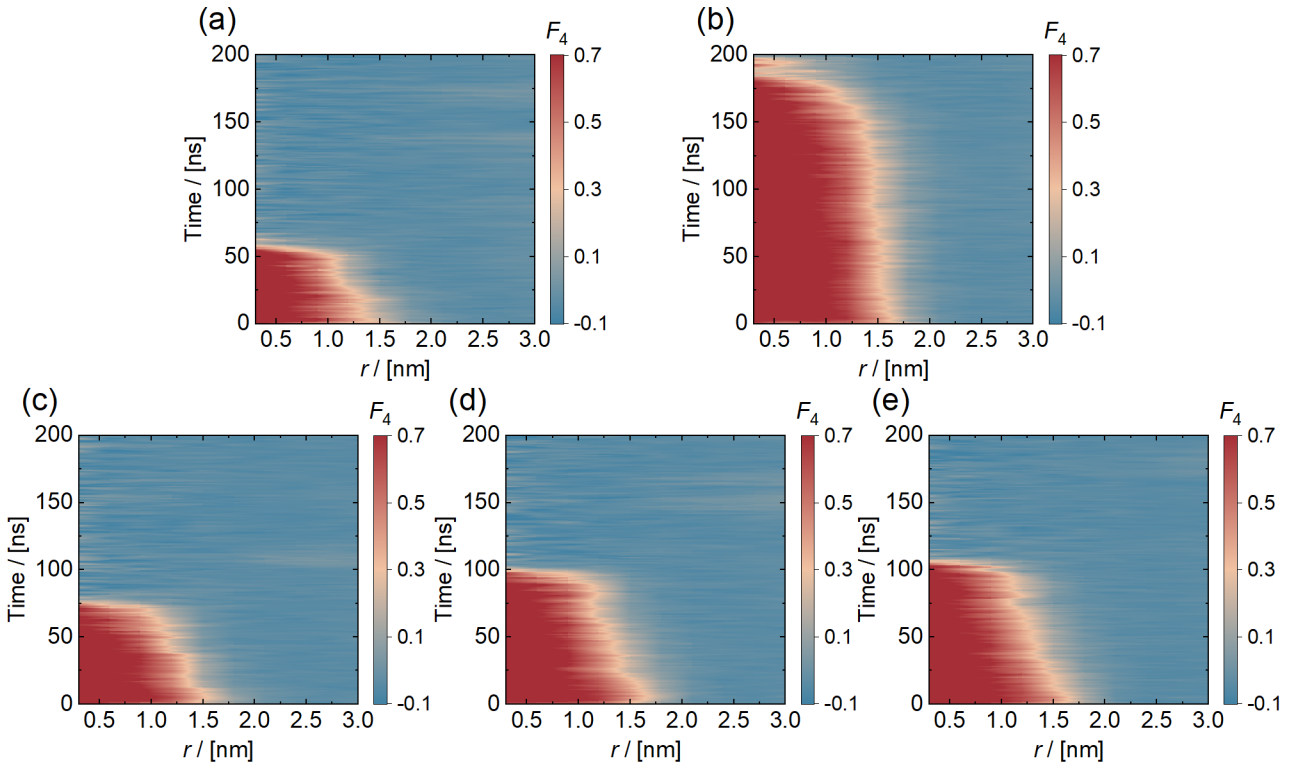

Figure S18. Time evolution of the F_4 from the center of the $D_{4.5}$ hydrate nanoparticle for the NP_{3THF} repeated systems, *i.e.*, (a) Run1, (b) Run2, (c) Run3, (d) Run4, and (e) Run5. The r = 0 nm represents the center of the hydrate nanoparticle, while sampling was averaged for 1 ns.

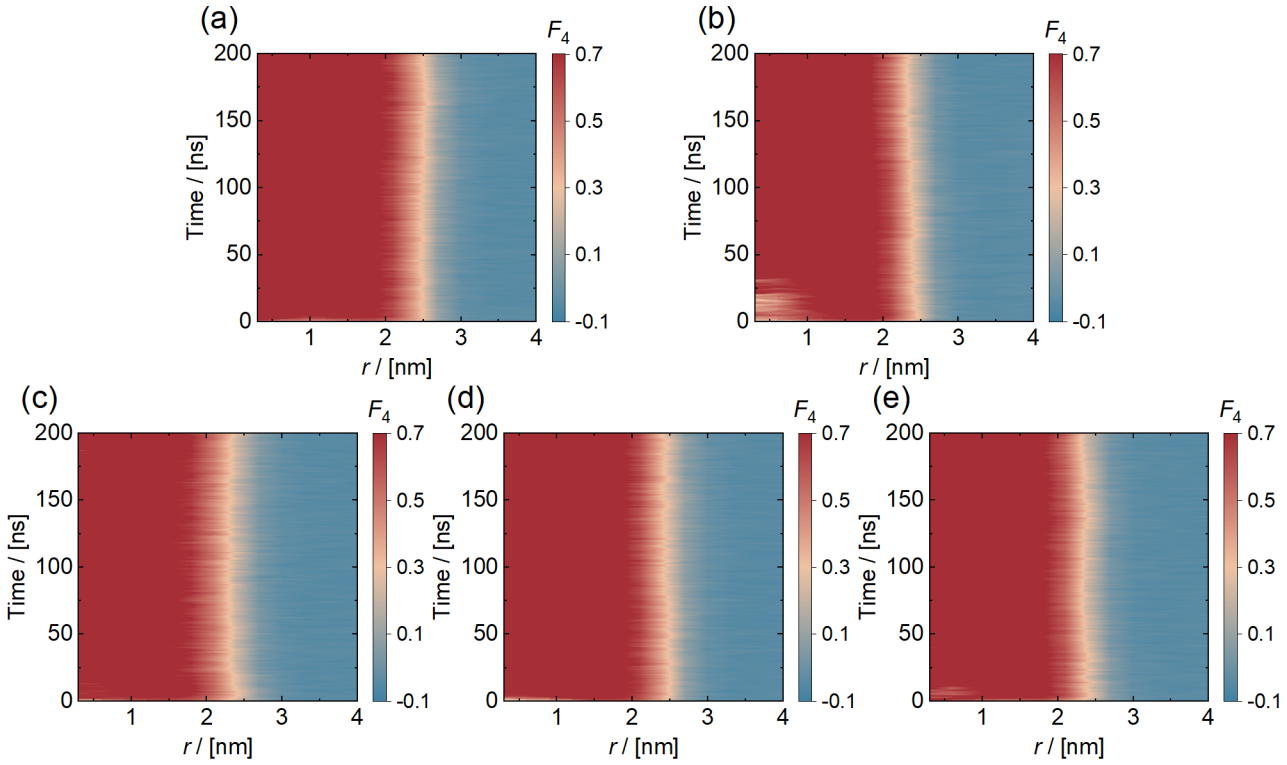

Figure S19. Time evolution of the F_4 from the center of the D_6 hydrate nanoparticle for the NP_{3THF} repeated systems, *i.e.*, (a) Run1, (b) Run2, (c) Run3, (d) Run4, and (e) Run5. The r = 0 nm represents the center of the hydrate nanoparticle, while sampling was averaged for 1 ns.

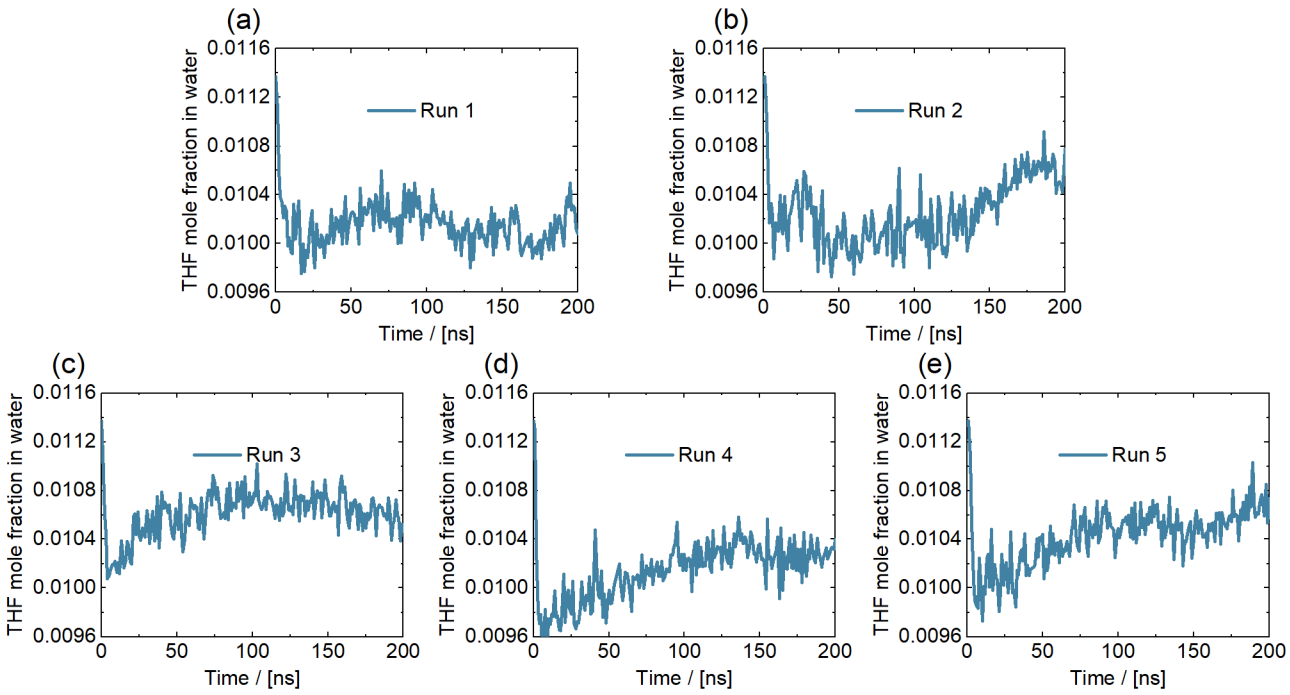

Figure S20. Time evolution of the THF mole fraction in water for the NP_{3THF} repeated systems, *i.e.*, (a) Run1, (b) Run2, (c) Run3, (d) Run4, and (e) Run5.

S3. Supporting Videos

Video S1. The coarsening process of THF hydrates for the NP_{2THF} system. THF is displayed as cyan (C atom) and red (O atom). Bonds of different colours represent seven types of hydrate cages, *i.e.*, green for 5^{12}, and orange for $5^{12}6^4$.

Video S2. The coarsening process of THF hydrates for the NP_{3THF} system. THF is displayed as cyan (C atom) and red (O atom). Bonds of different colours represent seven types of hydrate cages, *i.e.*, green for 5^{12}, and orange for $5^{12}6^4$.

S4. Supporting Reference

[1] Abraham MJ, Murtola T, Schulz R, Páll S, Smith JC, Hess B, et al. GROMACS: High performance molecular simulations through multi-level parallelism from laptops to supercomputers. SoftwareX. 2015;1:19-25.

[2] Abascal JL, Sanz E, Garcia Fernandez R, Vega C. A potential model for the study of ices and amorphous water: TIP4P/Ice. J Chem Phys. 2005;122:234511.

[3] Bussi G, Donadio D, Parrinello M. Canonical sampling through velocity rescaling. J Chem Phys. 2007;126:014101.

[4] Berendsen HJC, Postma JPM, Vangunsteren WF, Dinola A, Haak JR. Molecular-Dynamics with Coupling To an

External Bath. J Chem Phys. 1984;81:3684-3690.

[5] Nosé S. A Molecular-Dynamics Method for Simulations in the Canonical Ensemble. Mol Phys. 1984;52:255-268.

[6] Parrinello M, Rahman A. Crystal-Structure and Pair Potentials - a Molecular-Dynamics Study. Phys Rev Lett. 1980;45:1196-1199.

[7] Jacobson LC, Hujo W, Molinero V. Thermodynamic stability and growth of guest-free clathrate hydrates: a low-density crystal phase of water. J Phys Chem B. 2009;113:10298-10307.

[8] Potoff JJ, Siepmann JI. Vapor–liquid equilibria of mixtures containing alkanes, carbon dioxide, and nitrogen. AlChE J. 2001;47:1676-1682.